# *Minor Impact of Ligand Shell Steric Profile on Colloidal Nanocarbon Catalysis*

# The Minor Impact of Ligand Shell Steric Profile on Colloidal Nanocarbon Catalysis

Sterling B. Chu, Tomohiro Fukushima†, and Yogesh Surendranath*

Department of Chemistry, Massachusetts Institute of Technology, 77 Massachusetts Avenue, Cambridge, Massachusetts 02139

**ABSTRACT:** The catalytic activity of a colloidal nanoparticle is typically inhibited by the very capping agents that are required to maintain colloidal stability and catalyst dispersion. However, the relative importance of steric contributions to the observed attenuation in catalytic activity is poorly understood. Herein, we prepare colloidal graphitic carbon nanoparticles featuring covalent amide linkages to aliphatic surface capping agents of varying length. Using aerobic benzylamine oxidation as a test reaction, we find that the steric profile of the ligand shell plays a negligible role in suppressing catalytic activity relative to chemisorption interactions that alter the surface chemistry of the catalyst. The work suggests that heterostructured nanoparticles that provide distinct surface sites for ligand binding and substrate activation should allow for high colloidal stability and robust catalytic activity.

Colloidal nanoparticles are a diverse class of materials that have found numerous applications in areas such as biological sensing,[1,2] optoelectronics,[3,4] and energy conversion.[5,6] The high surface-area-to-volume ratio of nanomaterials makes them particularly attractive for catalytic applications as well. In this regard, colloidal nanoparticles could serve as a valuable bridge between traditional heterogeneous catalysis at extended solids and homogenous catalysis by small molecules.[7] In addition to displaying electronic structures that lie in between those of discrete molecules and bulk extended solids,[8,9] when dispersed in solution as stable colloids, nanoparticles are free to diffuse, allowing for rapid mass transport and straightforward measurement and modeling of the kinetics of catalytic reactions.[10–12]

Despite the potential promise of colloidal nanomaterials in connecting homogeneous and heterogeneous catalysis, the broad application of nanocolloids in catalysis has been impeded by their generally poor activity. The catalytic inertness of most colloidal nanomaterials has primarily been attributed to the capping agents that are invariably required for colloidal stability.[13–15] Currently, the mechanisms by which these capping agents inhibit catalysis remain largely unknown,[16,17] impeding the rational design of surface modification strategies or specialty surfactants that confer both colloidal stability *and* robust catalytic activity.

Prototypical capping agents typically consist of a polar head group that binds to the surface and a long aliphatic chain that provides colloidal stability owing to its high conformational entropy.[18] Thus, the capping agents could inhibit catalysis via two principal mechanisms. First, binding of the head-group to the surface may serve to poison catalytic active sites. Second, the ensemble of long aliphatic chains on the surface may serve to inhibit substrate access to surface active sites, imposing a steric restriction on catalysis. As each of these modes of catalyst deactivation calls for different remedies, parsing between these steric and surface poising effects is essential for developing high-performance colloidal nanocatalysts. However, the highly dynamic surface chemistry of most nanomaterials[19–21] makes it difficult, if not impossible, to dramatically alter the structure (e.g. chain length, functional groups) of the capping agent without simultaneously varying other key attributes of the material (e.g. surface ad-atom population, particle size, exposed facets, capping agent surface density).

To unambiguously parse the relative contributions of each mechanism to the observed catalytic activity of the nanomaterial, we exploit the covalent surface chemistry of graphitic carbon nanomaterials. Graphitic carbon surfaces contain a variety of oxidic functional groups, including quinones, ketones, phenols, lactones, and carboxylic acids,[22,23] which display well-documented and orthogonal chemical reactivity. Herein, we utilize classical amide formation reactions to install capping agents of varying chain lengths to surface carboxylic acid sites on Monarch 1300 carbon black. This surface treatment generates stable colloids that remain catalytically active for the aerobic oxidation of primary amines. Using the aerobic oxidation of benzylamine to *N*-benzyl-1-phenylmethanimine as a test reaction, we show that the capping ligand length negligibly impacts the rate of catalysis suggesting that, for linear aliphatic ligands, the ligand shell imposes minimal steric encumbrance on colloidal nanocatalysis.

**Scheme 1.** Native carboxylic acid sites on graphitic carbon nanoparticles are functionalized using primary amines of varying chain lengths to yield dispersible carbon nanocolloids. The image on the right shows **4** dispersed in tetrahydrofuran.

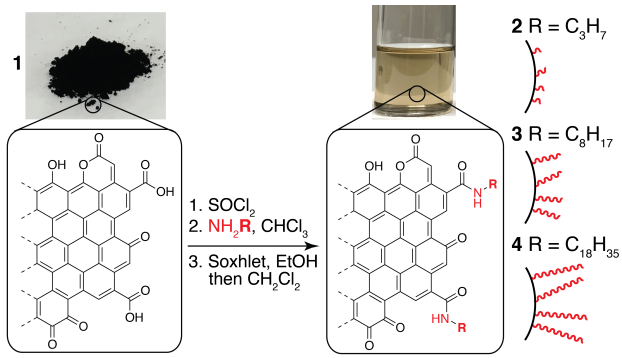


Colloidal graphitic-carbon nanoparticles were prepared by treating dried Monarch 1300 carbon black (**1**) (Cabot) with neat thionyl chloride under an $N_2$ atmosphere followed by treatment with propylamine, octylamine, or oleylamine in chloroform to generate colloidal nanoparticles **2**, **3**, and **4**, respectively (**Scheme 1**). The resulting material was washed exhaustively via Soxhlet extraction with ethanol followed by dichloromethane. The resulting powders were dried *in vacuo* to furnish the functionalized graphitic-carbon nanoparticles (see SI for complete synthetic details). Combustion analysis of the functionalized materials reveals an increase in N content of ~1 wt% relative to the native Monarch 1300 (**Table S1**), which is in line with the incorporation of nitrogen moieties onto the graphitic carbon surface. Using this value, along with the reported BET surface area of Monarch 1300 of 530 $m^2\ g^{-1}$,[24] we estimate similar capping agent densities of 0.9±0.1 ligands $nm^{-2}$ for materials **2**, **3**, and **4** (see SI for details of surface density calculation). Notably, this ligand density is comparable to the surface ligand density found for thiolate-capped gold nanoparticles[25] and semiconductor nanocrystals,[26,27] suggesting that the steric effects probed here are relevant to a wide variety of nanomaterials. Together, the data establish that this simple synthetic procedure generates functionalized graphitic carbons with similar surface coverages of capping agents irrespective of their aliphatic chain length. This ability to the tune the structure of the capping agent without altering its surface concentration is in stark contrast to what has been observed for metal and semiconductor nanocrystals, where ligand binding equilibria lead to higher surface densities for shorter chain length aliphatic ligands.[25] The ability to independently control these parameters enables the systematic studies described below.

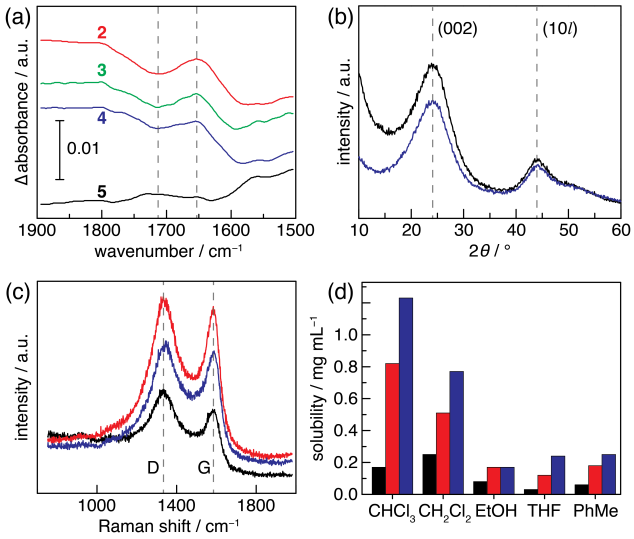


**Figure 1.** Difference infrared spectra (a) of modified graphitic carbon nanocolloids versus the absorbance spectrum of native Monarch 1300 (**1**). Powder X-ray diffraction patterns (b) of 002 and 10*l* reflections of **1** (black) and **4** (blue). Raman spectra (c) of **1** (black), **2** (red), and **4** (blue) recorded with 532 nm excitation. Masses of **1** (black), **2** (red), and **4** (blue) that remain suspended in a variety of solvents (d) following centrifugation at 4000 rpm for 5 minutes.

In order to probe the surface chemistry of the resulting functionalized material, we examined all samples via ATR infrared spectroscopy (**Figures 1a** and **S1**). A control sample was prepared by treating **1** with thionyl chloride to install acyl chloride surface moieties and then treating with water to hydrolyze these groups, thereby regenerating the surface carboxylic acid groups. This sequence generates sample **5**, which is expected to display equivalent surface chemistry to the unmodified carbon, **1**. Indeed, the IR difference spectrum between **1** and **5** shows a featureless background between 1900 and 1500 $cm^{-1}$ (**Figure 1a,** black), indicating that the thionyl chloride treatment does not introduce any gross changes to the surface chemistry of the carbon. However, difference spectra between **2**, **3**, and **4** (**Figure 1a**) and the native carbon display a broad bleach at 1710 $cm^{-1}$, suggesting a loss of carboxylic acid functionalities. Moreover, the functionalized materials display increased IR absorbance at 1650 $cm^{-1}$, in line with the installation of new surface amide functional groups.[28] While we cannot unambiguously rule out imine formation reactions on the surface, these data nonetheless suggest that this treatment serves to transform surface carboxylate moieties into amides, thereby covalently linking the capping agent to the carbon surface.

The surface ligation protocol employed here also preserves the bulk structure of the carbon material. Powder X-ray diffraction patterns of **1** and **4** (**Figure 1b**) reveal broad reflections corresponding to the 002 and 10*l* planes of graphite.[30] Scherrer analysis of the broadening in these peaks reveals that both materials display crystalline domain sizes of 1.3 nm for the out-of-plane (002) reflections and 3.6 nm for the in-plane (10*l*) reflections. Defect densi-

ties in these graphitic carbon nanoparticles were investigated by Raman spectroscopy.[31] **Figure 1c** shows the G-band (1580 $cm^{-1}$) and D-band (1330 $cm^{-1}$) resonances for **1**, **2**, and **4**. The G-band arises from the Raman-active $E_{2g}$ vibronic mode corresponding to in-plane vibrations, whereas the D-band arises from defects or disorder in the basal planes.[32,33] The relative intensity ($I_D/I_G$) of these bands for all of the carbon materials examined here remains constant (1.1±0.1), indicating that this synthetic method does not dramatically alter the defect density of the bulk material. Together, these data establish that surface functionalization does not dramatically alter the bulk structure of the graphitic carbon host.

Surface functionalization of graphitic-carbon nanoparticles significantly increases their colloidal solubility in a variety of organic solvents. Colloidal solubility was measured by dispersing particles in a particular solvent, centrifuging at 4000 rpm for 5 minutes, and then evaporating 10 mL of the supernatant to determine the mass of the suspended colloids (**Figure 1d**). Consistent with the general observation for colloidal semiconductor and metal nanoparticles, we observe that longer aliphatic chain lengths endow the material with greater colloidal solubility. Furthermore, measurements of the hydrodynamic radii of the suspended carbon colloids by dynamic light scattering reveal a tighter distribution for **4** (**Figure S2**) than for **1** (**Figure S3**), suggesting better dispersibility and greater resistance to agglomeration.

**Scheme 2.** Colloidal carbon catalyzed aerobic oxidation of benzylamine to *N*-benzyl-1-phenylmethanimine.

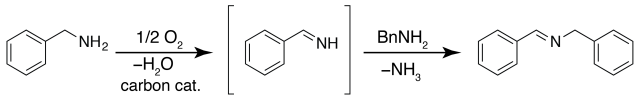


The aerobic oxidation of benzylamine to *N*-benzyl-1-phenylmethanimine serves as an ideal test reaction for examining the impact of capping agent structure on catalytic rate. Carbon surfaces are known to be populated with surface quinone moieties,[22,23] and quinone-based molecular catalysts are known to mediate the aerobic oxidation of primary amines with excellent selectivity.[34,35] Similar reactivity has also been reported for graphene oxide catalysts,[36] leading us to postulate that graphitic carbon colloids could also mediate this conversion. Indeed, as-received Monarch 1300 catalyzes the aerobic oxidation of benzylamine with selective formation of *N*-benzyl-1-phenylmethanimine (**Scheme 2** and **Figure S4**). Importantly, no product formation was observed under anaerobic conditions (**Figure S5a**) or in the absence of the carbon catalyst (**Figure S5b**), indicating that $O_2$ is the terminal oxidant and that the carbon surface is catalyzing the transformation. Molecular oxygen can serve as a two-electron oxidant, generating $H_2O_2$, or as a four-electron oxidant, generating $H_2O$. While we are unable to detect any $H_2O_2$ in the reaction mixture following a catalytic run (**Figure S6**), we cannot rule out a mechanistic sequence that initially generates $H_2O_2$ followed by rapid disproportionation to $O_2$ and $H_2O$ under the reaction conditions. Notably, whereas many molecular systems require a co-catalyst to regenerate the active quinone upon substrate oxidation,[37] the carbon surface simultaneously catalyzes $O_2$ reduction and amine oxidation.

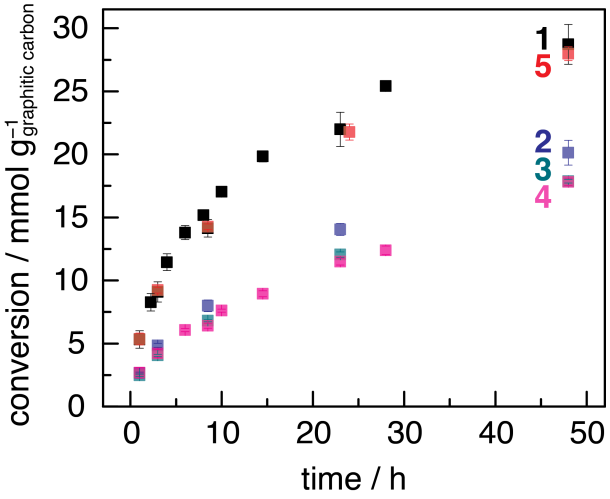


**Figure 2.** Time course of benzylamine conversion to *N*-benzyl-1-phenylmethanimine by aerobic oxidation catalyzed by 0.1 g of **1** (black), **2** (blue), **3** (green), **4** (pink), or **5** (red) in dry THF at 60 °C under 1 atm $O_2$. Data are normalized to mass loading of graphitic carbon (discounting the mass contributed by the aliphatic ligands in **2**, **3**, and **4**). Data normalized to the total carbon loading are plotted in **Figure S7**.

Using this test reaction, we monitored the rate of product, *N*-benzyl-1-phenylmethanimine, formation over time for all of the carbon samples, **1-5**. All catalytic runs were performed in dry THF at 60 °C under 1 atm $O_2$ with periodic quantification of product formation via $^1$H NMR spectroscopy of reaction aliquots (**Figure 2**). Samples **1** and **5** display similar conversion rates, indicating that the thionyl chloride treatment does not alter the material's intrinsic catalytic performance. Based on the hypothesis that the catalytic activity of the carbon arises from quinone surface groups,[34,35,37] one might expect that irreversible amidation of carboxylic acid surface sites would serve to retain the majority of the catalytic activity of the carbon sample. However, incorporation of capping ligands, irrespective of their length, leads to an ~2-fold decrease in reaction rate. While the origin of this suppression remains unknown at this time, we postulate that the decreased surface concentration of Brønsted acidic groups may retard the rate of proton transfer steps necessary for $O_2$ reduction and substrate oxidation. Given that these effects are expected to be the same for all functionalized colloids, we now compare their activities as a function of ligand length to isolate the impact of the ligand shell steric profile on catalysis. Amongst the functionalized nanocarbons, varying the capping agent length from $C_3$ to $C_{18}$ results in a 25 ± 4 percent additional decrease in observed conversion at the same mass-loading of the carbon (**Figure S7**). This can be explained in large part by the increased mass fraction of the inert aliphatic chains that do not contribute to catalysis. Elemental analysis suggests that the $C_3$ material (**2**) consists of 4 wt% capping ligands while the ligands represent 18 wt% of the $C_{18}$ material (**4**).

Thus, the variation in substrate conversion after 48 hours is modest, ~10%, upon taking into account the differing graphitic mass loadings (**Figure 2**). This indicates a similar specific activity for all functionalized materials despite a dramatic variation in capping agent length. These results establish that while surface functionalization leads to a pronounced decrease in catalytic activity, the chain length of the capping ligand plays a minor role in the observed attenuation.

In conclusion, we have utilized covalent amide functionalization of graphitic carbon surfaces to generate catalytically-active, colloidally-dispersible nanocarbons. The irreversibility and specificity of the amide formation reaction allows for systematic tuning of the capping agent length without altering the surface concentration of the capping species. This has allowed us to parse, for the first time, the degree of steric encumbrance imposed by linear aliphatic ligand shells on the catalytic activity of the nanocarbon. The relative invariance of the catalytic activity as a function of capping ligand length indicates that even very long $C_{18}$ capping ligands do not impose a substantial steric penalty. Given that the capping ligand densities we observe on carbon colloids are similar to the ligand densities observed on metal and semiconductor nanocrystals, our findings suggest that there is no intrinsic incompatibility between good colloidal stability and efficient colloidal catalysis. Indeed, these results suggest that a key to developing colloidally stable, highly active nanocatalysts is to synthesize heterostructured surfaces[38] that host capping ligand binding and catalysis at chemically distinct sites.

## ASSOCIATED CONTENT

### Supporting Information

The Supporting Information is available free of charge on the ACS Publications website.

Full experimental details, elemental analysis, full IR spectra, DLS of **1** and **4**, NMR time course data with internal standards, NMR time course data in the absence of catalyst or oxygen, and $^{31}$P NMR assay data for hydrogen peroxide. (PDF)

## AUTHOR INFORMATION


### Corresponding Author

* yogi@mit.edu

### Present Addresses

†Graduate School of Science, Nagoya University, Chikusa, Nagoya 464-8602, Japan


### Notes

The authors declare no competing financial interest.

## ACKNOWLEDGMENT


We gratefully acknowledge Amanda Stubbs for assistance with infrared spectroscopy measurements. T.F. thanks Dr. Dimitri Vaughn II for fruitful discussions on nanoparticle chemistry and Tomohiro Soejima for assistance on XRD measurements. This work was supported primarily by the MRSEC Program of the National Science Foundation under award number DMR – 1419807 and supported in part by the MIT Department of Chemistry through junior faculty funds for Y.S. T.F. was supported by a JSPS postdoctoral fellowship for research abroad.


## REFERENCES


(1) Bruchez Jr., M.; Moronne, M.; Gin, P.; Weiss, S.; Alivisatos, A. P. Semiconductor Nanocrystals as Fluorescent Biological Labels. *Science (80-. ).* **1998**, *281*, 2013–2016.

(2) Jun, Y.; Seo, J.; Cheon, J. Nanoscaling Laws of Magnetic Nanoparticles and Their Applicabilities in Biomedical Sciences. *Acc. Chem. Res.* **2008**, *41*, 179–189.

(3) Klimov, V. I.; Mikhailovsky, A. A.; Xu, S.; Malko, A.; Hollingsworth, J. A.; Leatherdale, C. A.; Eisler, H.-J.; Bawendi, M. G. Optical Gain and Stimulated Emission in Nanocrystal Quantum Dots. *Science (80-. ).* **2000**, *290*, 314–317.

(4) Talapin, D. V.; Lee, J.-S.; Kovalenko, M. V.; Shevchenko, E. V. Prospects of Colloidal Nanocrystals for Electronic and Optoelectronic Applications. *Chem. Rev.* **2010**, *110*, 389–458.

(5) Kalyanasundaram, K.; Gratzel, M. Interfacial Electron Transfer in Colloidal Metal and Semiconductor Dispersions and Photodecomposition of Water. *Coord. Chem. Rev.* **1986**, *69*, 57–125.

(6) Schmidt, T. J.; Noeske, M.; Gasteiger, H. A.; Behm, R. J.; Britz, P.; Brijoux, W.; Bönnemann, H. Electrocatalytic Activity of PtRu Alloy Colloids for CO and CO/H 2 Electrooxidation: Stripping Voltammetry and Rotating Disk Measurements. *Langmuir* **1997**, *13*, 2591–2595.

(7) Astruc, D.; Lu, F.; Aranzaes, J. R. Nanoparticles as Recyclable Catalysts: The Frontier between Homogeneous and Heterogeneous Catalysis. *Angew. Chemie Int. Ed.* **2005**, *44*, 7852–7872.

(8) Murray, C. B.; Norris, D. J.; Bawendi, M. G. Synthesis and Characterization of Nearly Monodisperse CdE (E = Sulfur, Selenium, Tellurium) Semiconductor Nanocrystallites. *J. Am. Chem. Soc.* **1993**, *115*, 8706–8715.

(9) Rossetti, R.; Nakahara, S.; Brus, L. E. Quantum Size Effects in the Redox Potentials, Resonance Raman Spectra, and Electronic Spectra of CdS Crystallites in Aqueous Solution. *J. Chem. Phys.* **1983**, *79*, 1086–1088.

(10) Li, Y.; Hong, X. M.; Collard, D. M.; El-Sayed, M. A. Suzuki Cross-Coupling Reactions Catalyzed by Palladium Nanoparticles in Aqueous Solution. *Org. Lett.* **2000**, *2*, 2385–2388.

(11) Schulz, J.; Roucoux, A.; Patin, H. Unprecedented Efficient Hydrogenation of Arenes in Biphasic Liquid–liquid Catalysis by Re-Usable Aqueous Colloidal Suspensions of Rhodium. *Chem. Commun.* **1999**, 535–536.

(12) Widegren, J. A.; Finke, R. G. A Review of Soluble Transition-Metal Nanoclusters as Arene Hydrogenation Catalysts. *J. Mol. Catal. A Chem.* **2003**, *191*, 187–207.

(13) Kuhn, J. N.; Tsung, C.-K.; Huang, W.; Somorjai, G. A. Effect of Organic Capping Layers over Monodisperse Platinum Nanoparticles upon Activity for Ethylene Hydrogenation and Carbon Monoxide Oxidation. *J. Catal.* **2009**, *265*, 209–215.

(14) Li, D.; Wang, C.; Tripkovic, D.; Sun, S.; Markovic, N. M.; Stamenkovic, V. R. Surfactant Removal for Colloidal Nanoparticles from Solution Synthesis: The Effect on Catalytic Performance. *ACS Catal.* **2012**, *2*, 1358–1362.

(15) De Roo, J.; Van Driessche, I.; Martins, J. C.; Hens, Z. Colloidal Metal Oxide Nanocrystal Catalysis by Sustained

Chemically Driven Ligand Displacement. *Nat. Mater.* **2016**, *15*, 517–521.
(16) Kwon, S. G.; Krylova, G.; Sumer, A.; Schwartz, M. M.; Bunel, E. E.; Marshall, C. L.; Chattopadhyay, S.; Lee, B.; Jellinek, J.; Shevchenko, E. V. Capping Ligands as Selectivity Switchers in Hydrogenation Reactions. *Nano Lett.* **2012**, *12*, 5382–5388.
(17) Stowell, C. A.; Korgel, B. A. Iridium Nanocrystal Synthesis and Surface Coating-Dependent Catalytic Activity. *Nano Lett.* **2005**, *5*, 1203–1207.
(18) Polte, J. Fundamental Growth Principles of Colloidal Metal Nanoparticles – a New Perspective. *CrystEngComm* **2015**, *17*, 6809–6830.
(19) Knauf, R. R.; Lennox, J. C.; Dempsey, J. L. Quantifying Ligand Exchange Reactions at CdSe Nanocrystal Surfaces. *Chem. Mater.* **2016**, *28*, 4762–4770.
(20) Anderson, N. C.; Hendricks, M. P.; Choi, J. J.; Owen, J. S. Ligand Exchange and the Stoichiometry of Metal Chalcogenide Nanocrystals: Spectroscopic Observation of Facile Metal-Carboxylate Displacement and Binding. *J. Am. Chem. Soc.* **2013**, *135*, 18536–18548.
(21) Morris-Cohen, A. J.; Vasilenko, V.; Amin, V. A.; Reuter, M. G.; Weiss, E. A. Model for Adsorption of Ligands to Colloidal Quantum Dots with Concentration-Dependent Surface Structure. *ACS Nano* **2012**, *6*, 557–565.
(22) McCreery, R. L. Advanced Carbon Electrode Materials for Molecular Electrochemistry. *Chem. Rev.* **2008**, *108*, 2646–2687.
(23) Boehm, H. P. Surface Oxides on Carbon and Their Analysis: A Critical Assessment. *Carbon N. Y.* **2002**, *40*, 145–149.
(24) O'Reilly, J. M.; Mosher, R. A. Functional Groups in Carbon Black by FTIR Spectroscopy. *Carbon N. Y.* **1983**, *21*, 47–51.
(25) Hinterwirth, H.; Kappel, S.; Waitz, T.; Prohaska, T.; Lindner, W.; Laemmerhofer, M. Quantifying Thiol Ligand Density of Self-Assembled Monolayers on Gold Nanoparticles by Inductively Coupled Plasma-Mass Spectrometry. *ACS Nano* **2013**, *7*, 1129–1136.
(26) Valdez, C. N.; Schimpf, A. M.; Gamelin, D. R.; Mayer, J. M. Low Capping Group Surface Density on Zinc Oxide Nanocrystals. *ACS Nano* **2014**, *8*, 9463–9470.
(27) Hens, Z.; Martins, J. C. A Solution NMR Toolbox for Characterizing the Surface Chemistry of Colloidal Nanocrystals. *Chem. Mater.* **2013**, *25*, 1211–1221.
(28) Sorrell, T. N. *Organic Chemistry*; 2nd ed.; University Science Books: Sausalito, 2006.
(29) Gomes, R.; Hassinen, A.; Szczygiel, A.; Zhao, Q.; Vantomme, A.; Martins, J. C.; Hens, Z. Binding of Phosphonic Acids to CdSe Quantum Dots: A Solution NMR Study. *J. Phys. Chem. Lett.* **2011**, *2*, 145–152.
(30) Li, Z. Q.; Lu, C. J.; Xia, Z. P.; Zhou, Y.; Luo, Z. X-Ray Diffraction Patterns of Graphite and Turbostratic Carbon. *Carbon N. Y.* **2007**, *45*, 1686–1695.
(31) Ferrari, A. C.; Basko, D. M. Raman Spectroscopy as a Versatile Tool for Studying the Properties of Graphene. *Nat. Nanotechnol.* **2013**, *8*, 235–246.
(32) Reich, S.; Thomsen, C. Raman Spectroscopy of Graphite. *Philos. Trans. R. Soc. A Math. Phys. Eng. Sci.* **2004**, *362*, 2271–2288.
(33) Tuinstra, F.; Koenig, J. L. Raman Spectrum of Graphite. *J. Chem. Phys.* **1970**, *53*, 1126–1130.
(34) Wendlandt, A. E.; Stahl, S. S. Bioinspired Aerobic Oxidation of Secondary Amines and Nitrogen Heterocycles with a Bifunctional Quinone Catalyst. *J. Am. Chem. Soc.* **2014**, *136*, 506–512.
(35) Wendlandt, A. E.; Stahl, S. S. Chemoselective Organocatalytic Aerobic Oxidation of Primary Amines to Secondary Imines. *Org. Lett.* **2012**, *14*, 2850–2853.
(36) Khalili, D.; Banazadeh, A. R. Graphene Oxide as a Heterogeneous Reagent Promoted Synthesis of 2-Substituted 1,3-Benzazoles in Water. *Bull. Chem. Soc. Jpn.* **2015**, *88*, 1693–1706.
(37) Wendlandt, A. E.; Stahl, S. S. Quinone-Catalyzed Selective Oxidation of Organic Molecules. *Angew. Chemie Int. Ed.* **2015**, *54*, 14638–14658.
(38) Buck, M. R.; Bondi, J. F.; Schaak, R. E. A Total-Synthesis Framework for the Construction of High-Order Colloidal Hybrid Nanoparticles. *Nat. Chem.* **2011**, *4*, 37–44.

Authors are required to submit a graphic entry for the Table of Contents (TOC) that, in conjunction with the manuscript title, should give the reader a representative idea of one of the following: A key structure, reaction, equation, concept, or theorem, etc., that is discussed in the manuscript. Consult the journal's Instructions for Authors for TOC graphic specifications.

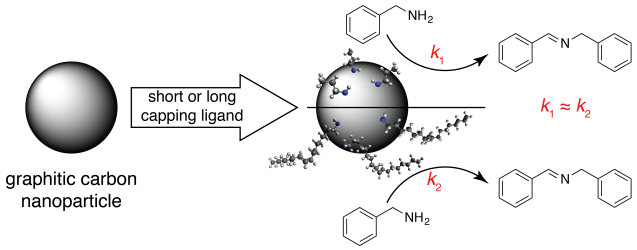


Insert Table of Contents artwork here